H-bonds/ionic coordination switching for fabrication of highly oriented cellulose hydrogels

Shuai Zhou, Kechun Guo, Danil Bukhvalov, Wenzhuo Zhu, Jian Wang, Wen Sun and Ming He*

Video_S1.mp4

Experimental Section

Materials. Cellulose (cotton linter pulp, α-cellulose content beyond 96.0 wt%) was obtained from Nantong Cellulose Fibers Company. Zinc chloride ($ZnCl_2$, 99.0 wt %) and calcium chloride ($CaCl_2$, 99.0 wt %) were provided by Nanjing Reagent Company. All of the reagents were used as received unless otherwise noted.

Pre-made cellulose gel. 9.87 g of $ZnCl_2$ and 0.3g of $CaCl_2$ were dissolved in 3.63 g of deionized water at 75 °C. Then, 0.2 g of cotton cellulose was dissolved in $ZnCl_2$/$CaCl_2$ solution at 75 °C. 2.5g of water was added at 90 °C and the mixture was stirred evenly and remove air bubbles by ultrasonic. Cellulose solution was poured into the mold and cooled to room temperature to get cellulose gel (initial gel). The initial sample was soaked in a 40wt % $CaCl_2$ solution for 6 hours, where the $CaCl_2$ solution was changed several times until the exchange reached equilibrium to obtain an H_2O-l-0 gel.

Preparation of perfectly highly aligned gels

Both ends of a sample (H_2O-1-0 gel) of ~11 mm width and ~4 mm thickness were clamped. The distance between the two clamps was ~ 45mm. The gel was equilibrated in 500ml of water for 240 min to get H_2O-1-240 gel. During the process, because of the two ends of the gel fixed, the width and thickness of the hydrogel will shrink and the cellulose chains are oriented along the length direction. Ca-1 gel was prepared by soaking H_2O-1-240min gel in 150 ml of 40 wt % $CaCl_2$ solution for 10 min. Then the Ca-1 gel was soaked in 300ml of water for 10 min to obtain H_2O-2 gel. H_2O-1 to H_2O-8 gels and Ca-1 to Ca-8 gels were prepared by repeating the above process. Note that except for the H_2O-1-0 process which is 240min, the other processes are 10min.

Preparation of gels with bilayer structure

Both ends of H_2O-1-0 gel (~10 mm width, ~3 mm thickness) were clamped and the distance between the two clamps was ~ 85mm. The half of the gel was soaked in water and the other half was left in

the air along the width direction. After soaked in 150 ml of 40 wt % $CaCl_2$ solution for 10min, the gel was taken out of the clamps and the clamped part was cut off. Then repeating the above process of preparing anisotropic gel, the only difference was that the sample did not need to be clamped. Finally, the gels with bilayer structure were achieved.

Preparation of gels with gradient anisotropy

Both ends of H_2O-1-0 gel of ~45 mm width and ~2 mm thickness were clamped and the distance between the two clamps was ~ 70mm. The gel was soaked in water with a height of about 5mm. Then the height of water increased by 5mm every 5 min until the height of water increased to 30 mm. Then the gel was soaking in 40 wt % $CaCl_2$ solution for 10min to obtain the gradient anisotropic gel.

Structure characterization. The gel was in-situ observed under orthogonally polarized light and related digital photos were taken by camera. UV-visible spectroscopy analysis and transmittance spectra of the gels was carried out on an Ocean Optics 2000+ UV-Vis/NIR spectrophotometer in conjunction with a polarizing microscope. The morphology of cross-section surface was observed by cold field scanning electron microscopy (FSEM) (Regulus 8100) with a voltage of 2 kV. Before testing, the sample was fractured in liquid nitrogen to obtain its cross section. Fourier transform infrared (FT-IR) spectra were gained from FT-IR spectrometer (Brucker VERTEX 80V) with an attenuated total reflection (ATR) mode. X-ray diffraction (XRD) experiments was performed by Rigaku Ultima IV. The samples were scanned with 2θ from 5° to 60° and the scanning speed was 5° /min. The small-angle X-ray scattering (Bruker-AXS NanoSTAR) system was equipped with a 30W microfocus Incoatec IμSCu source and an area detector (Vantec-2000). The generator operated at 40 kV and 20 μA, and the detector-to-sample distance was 105 nm. The data acquisition time was 1800 s per sample, and scattering angles ranged from 0.044° to 4.4°.

Calculation of birefringence[1, 2]. The light emitted from the sample has a phase difference δ given by equation (1), where d is the thickness of the sample and λ is the wavelength of the light. The transmittance of cross ($T_\perp$) and parallel ($T_\parallel$) analyzers expressed by equations (2) and (3), where ϕ is the angle between the compression orientation and the polarization axis of the polarizer, fixed at 45°, δ Is the phase difference between polarizations. The birefringence (Δn) in equations (4) and (5)

can be derived from equations (1), (2) and (3), where k is a non-negative integer describing the order of samples. Choose different values of k to obtain trace plots that varies with wavelength and transmittance. Note in each trace plot, only the near-horizontal part is meaningful, and the connected traces in the horizontal part correctly reflect the birefringence of the sample.

$$\delta = \frac{2\pi d \Delta n}{\lambda} \quad \textbf{(1)}$$

$$T_{\perp} = \sin(2\phi)\sin^2\frac{\delta}{2} \quad \textbf{(2)}$$

$$T_{\parallel} = \sin(2\phi)\cos^2\frac{\delta}{2} \quad \textbf{(3)}$$

$$\Delta n = \frac{\lambda}{2\pi d}\left[k\pi + 2\tan^{-1}\sqrt{\frac{T_{\perp}}{T_{\parallel}}}\right] \quad \boldsymbol{k} = \textbf{0, 2, 4, …} \quad \textbf{(4)}$$

$$\Delta n = \frac{\lambda}{2\pi d}\left[(k+1)\pi - 2\tan^{-1}\sqrt{\frac{T_{\perp}}{T_{\parallel}}}\right] \quad \boldsymbol{k} = \textbf{1, 3, 5, …} \quad \textbf{(5)}$$

In addition, the Cauchy formula normally simplified as the Sellmeier dispersion equation was used to express the dispersion effect:

$$\Delta n = C + \frac{D}{\lambda^2} \quad \textbf{(6)}$$

Note that C and D are two constants. The horizontal intersection trajectory was first obtained in equations 4 and 5, and relying on the fitting of the least square method, the C and D values that were closest to the experimental results can be obtained.

Mechanical test. Tensile test of all samples ~30 mm in length was performed at room temperature by electromechanical universal testing machine (CMT850) and the stretching rate was 10 mm/min.

DFT calculation of Ca^{2+} concentration on the stability of cellulose gel

At the first step we have performed calculations of infinite chain in vacuum-like conditions. This means that other chains is parallel but remoted on more than 2 nm from this chain therefore no interactions between the chains. At the second step we put water molecules one per hydrophilic center (–OH and –O–). At the next step we performed optimization of atomic position of hydrated single chains. The next step is to decrease the distances between chains within periodic boundary

conditions until overlap of van der Waals radii of utmost atoms with further optimization of atomic position and lattice parameters. Note that for all considered structures initial lattice was tetragonal (all angles is 90 degrees) and almost hexagonal structure of hydrated cellulose appeared in result of self-consistent optimization. This significant transformation from initial tetragonal to final hexagonal structures demonstrates robust inter-chain forces in hydrated cellulose. At the next steps we put one Ca^{2+} in per supercell, then optimize atomic positions and lattice, then put second and until four Ca^{2+} in per supercell. Note that in result of the optimization Ca^{2+} not only influences positions of atoms in polymeric chains of cellulose but also reorders water around itself and nearest hydrophilic centers.

The density functional theory is to verify the assumed multiple effects of Ca^{2+} concentration. In the case of hydrated cellulose hexagonal patterns is less ordered (Fig. S1a), incorporation of minimal amount of Ca^{2+} does not provide formation of the cross-links because there is (i) rather large distance to –OH groups on other chains and (ii) Ca^{2+} have enough neighbors for coordination (Fig. S1b). Further load of Ca^{2+} leads to visible distortion of cellulose chains that decreases the distance between Ca^{2+} and –OH groups from other chains and also changes local coordination that provides appearance of some cross-links (Fig. S1c). When further exploring the mechanism of Ca^{2+} concentration affecting the structure of cellulose gel, it is proposed that the interaction between sugar ring and Ca^{2+} plays a key role. When load of Ca^{2+} is small oxygen groups on sugar rings something like swallow Ca^{2+} and water coordinated from above. When we increase amount of Ca^{2+}, cellulose chains are slightly elongated and some Ca^{2+} rises above sugar ring and also interacts with other chains and now water coordinates from sides. The result of the DFT model above explains the effect mechanism of Ca^{2+} concentration very well.

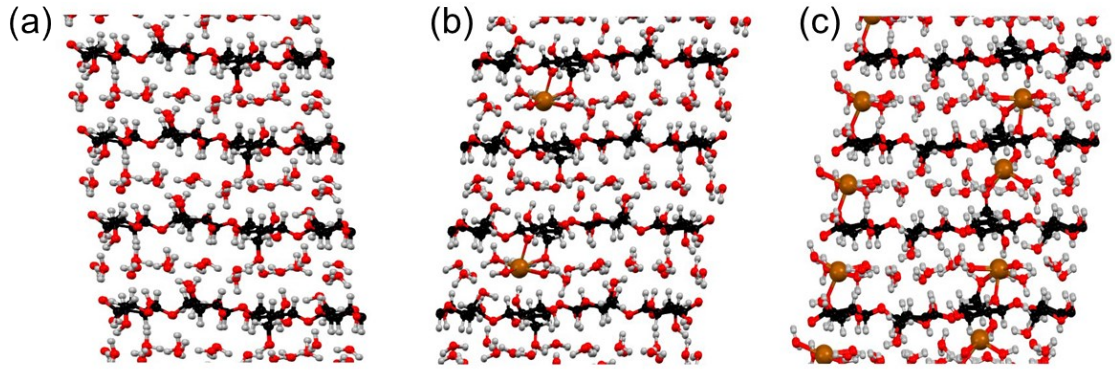

Fig. S1 Views across cellulose chain of optimized atomic structures of (a) hydrated cellulose, after introducing of (b) minimal and (c) maximal amount of Ca^{2+}.

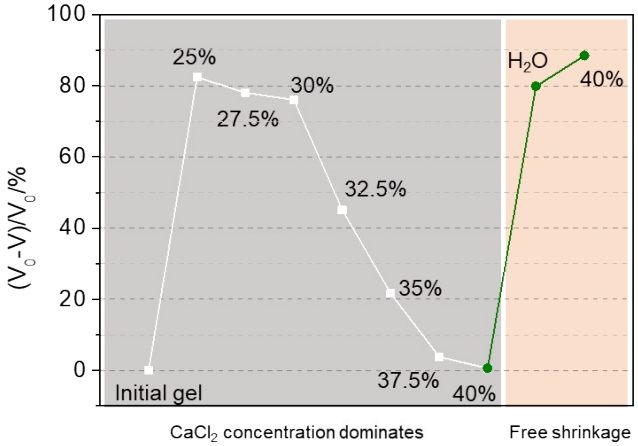

Fig. S2 Diagram of volume shrinkage rate corresponding to each stage in Fig. 1. Note: V_0 represents the volume of the initial gel, and V represents the volume of the corresponding stage.

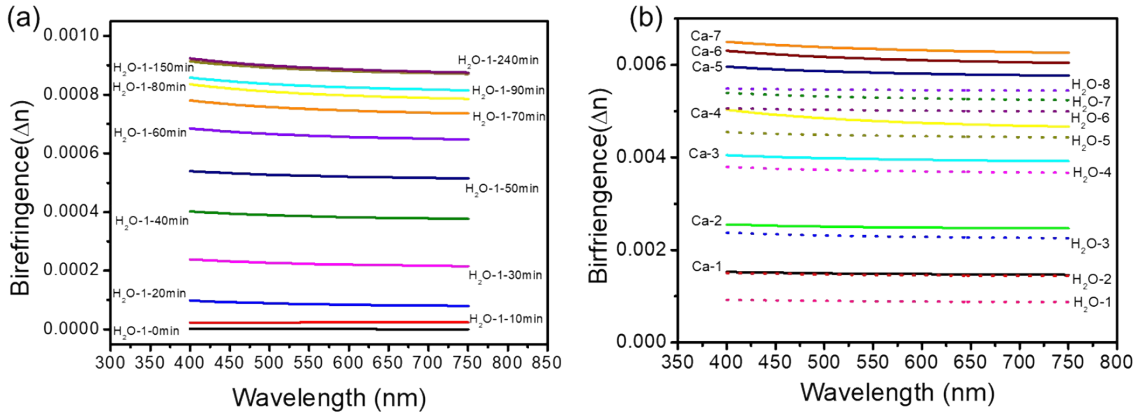

Fig. S3 (a) The birefringence at different wavelengths of the gel during primary regulation process estimated by fitting the Cauchy formula. (b) The birefringence at different wavelengths of the gel during secondary regulation

process estimated by fitting the Cauchy formula.

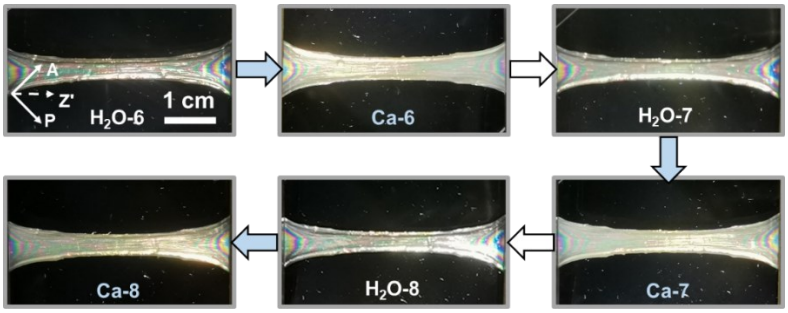

Fig. S4 The interference color change under multiple Ca^{2+}/H_2O exchange in secondary regulation (H_2O-6 to Ca-8 process). The polarization axis is at 45° to the confined length of the gel.

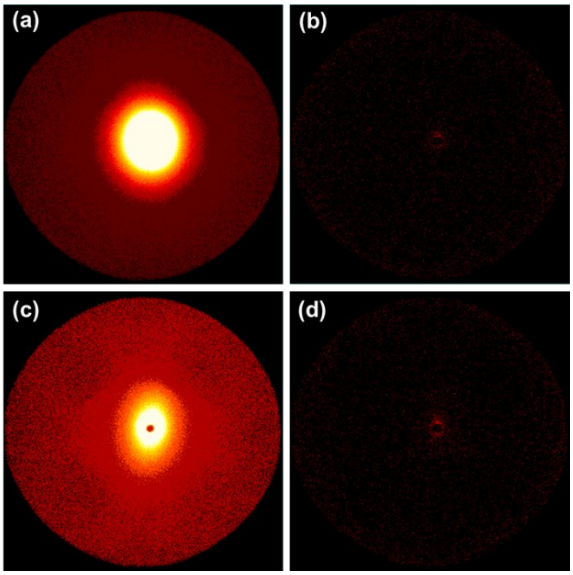

Fig. S5 2D SAXS results of (a) H_2O-1-240min gel, (b) Ca-1 gel, (c) H_2O-7 gel and Ca-7 gel

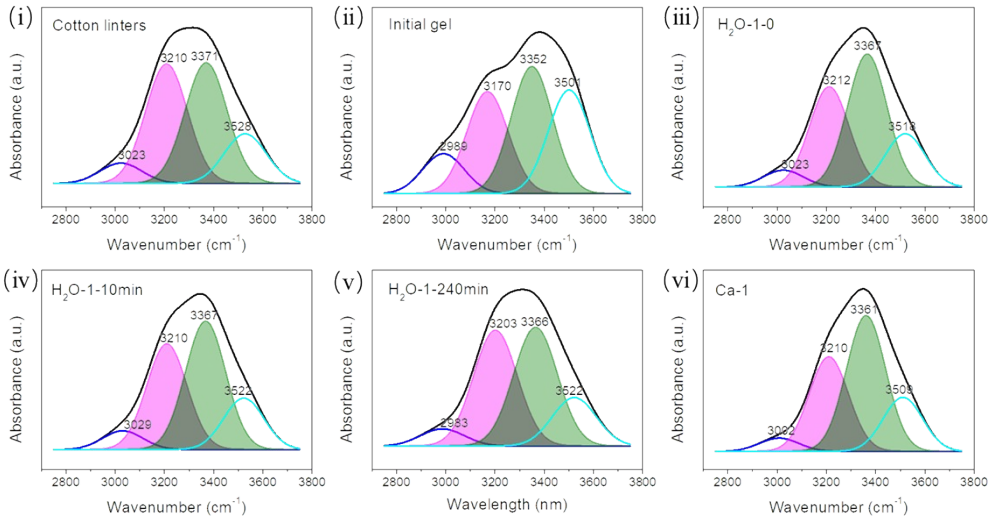

Fig. S6 FT-IR spectra with peak fitted by Gauss Amp to explore the transition of intermolecular H-bonds and intramolecular H-bonds during H_2O/Ca^{2+} exchange process. Note: the peak near 3360 cm^{-1} could belong to the intramolecular H-bonds of O3H···O5, while the peak near 3200 cm^{-1} could belong to the intermolecular H-bonds of

O6H···O3 and that between the cellulose –OH group and the strong bound water.

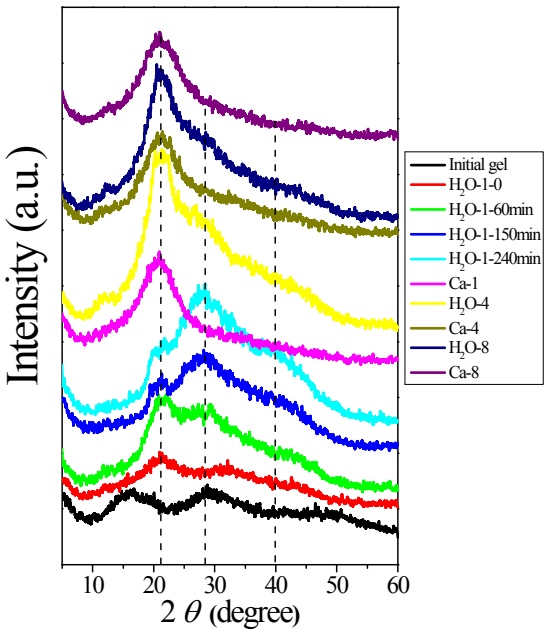

Fig. S7 XRD patterns for gels during H_2O/Ca^{2+} exchange process

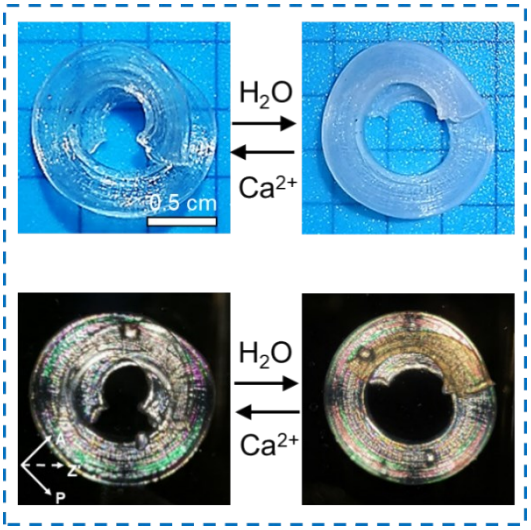

Fig. S8 The shape of the gel petal transformed to a ring by multiple H_2O/Ca^{2+} exchange processes. The shape and interference color change of the gel between transparency and opaque.

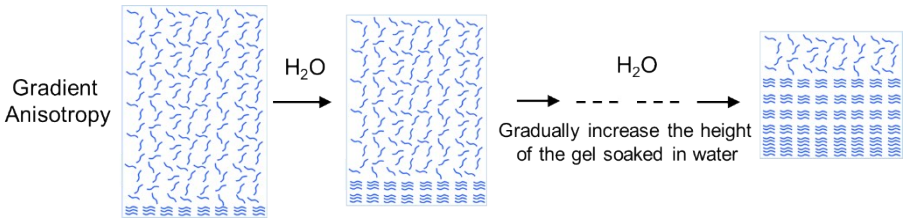

Fig. S9 Schematic diagram of the preparation of gradient anisotropic gel.

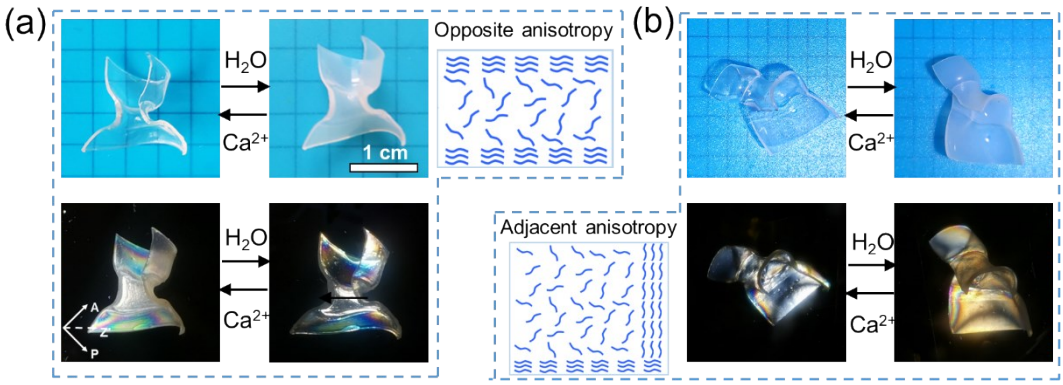

Fig. S10 (a) The gel with opposite anisotropic structure becomes a saddle-like structure due to asymmetric shrinkage. (b) The gel with adjacent anisotropic structure transforms into an irregular structure due to asymmetric shrinkage. Note that the change between transparent and opaque and the interference color change can be observed.

Table S1. Birefringence, water content and mechanical properties of samples under different preparation methods

Method description	Sample name	Sample description	Birefringence, Δn (10^{-3})	Water contents [wt%]	Fracture Stress [MPa]	Fracture Strain [%]	Modulus [MPa]
DCC method	50% DCC-alginate[3]	Pre-stretching ratios=0.5	~2.3×10^{-3}	~56 (after re-swollen in water)	~19.8	~51.1	~367.35
	CNC xerogels[4]	Pre-stretching ratios=10, W0/D0=32	~3.5×10^{-3}	–	~78	~15	–
Stretching	Cellulose nanocrystal-elastomer[1]	Elongation ratios =0.8	~2.5×10^{-3}	–	1.1 (original)	920 (original)	–
	Cellulose gels[5]	Elongation ratios =1	~5.5×10^{-3}	~68	~24	~42	~80
Ion diffusion induction	LC gel[6]	immersing in 0.5M $CaCl_2$ (Cp=1 wt%)	~8.8×10^{-5}	–	~0.03	~27	~0.14
	Ca-alginate hydrogels[7]	3wt% Alginate, 0.5M Ca^{2+}	~2nd or higher order (No Δn reported)	95.1	0.45	92	0.95
This work	H_2O-8	Without pre-stretching	~5.5×10^{-3}	~72	~8.66	~38.96	~18.28
	Ca-7	Without pre-stretching	~6.4×10^{-3}	~44	~6.47	~42.26	~15.29
Shear force	PDGI/PAAm gels[8]	C_{DGI}=0.2M, shear flow speed of 5 cm/s	~4×10^{-4}	–	~1.0	~90	~0.10
–	Knee ligaments[3]	–	–	60–70	13–46	11–44	65–447

1. O. Kose, A. Tran, L. Lewis, W. Y. Hamad and M. J. MacLachlan, *Nat. Commun.*, 2019, **10**, 510-516.
2. T. Hiratani, O. Kose, W. Y. Hamad and M. J. MacLachlan, *Mater. Horiz.*, 2018, **5**, 1076-1081.
3. M. T. I. Mredha, Y. Z. Guo, T. Nonoyama, T. Nakajima, T. Kurokawa and J. P. Gong, *Adv. Mater.*, 2018, **30**, 1704937-1704944.
4. H. Huang, X. Wang, J. Yu, Y. Chen, H. Ji, Y. Zhang, F. Rehfeldt, Y. Wang and K. Zhang, *ACS Nano*, 2019, **13**, 3867-3874.
5. M. T. I. Mredha, H. H. Le, T. Van Tron, P. Trtik, J. Cui and I. Jeon, *Mater. Horiz.*, 2019, **6**, 1504-1511.
6. Z. L. Wu, T. Kurokawa, D. Sawada, J. Hu, H. Furukawa and J. P. Gong, *Macromolecules*, 2011, **44**, 3535-3541.
7. M. T. I. Mredha, T. Van Tron, S.-G. Jeong, J.-K. Seon and I. Jeon, *Soft Matter*, 2018, **14**, 7706-7713.

8. M. A. Haque, G. Kamita, T. Kurokawa, K. Tsujii and J. P. Gong, *Adv. Mater.*, 2010, **22**, 5110–5114.